

Mapping the  $N = 40$  island of inversion: Precision mass measurements of neutron-rich Fe isotopes

W. S. Porter<sup>1,2,\*</sup>, B. Ashrafkhani,<sup>3</sup> J. Bergmann,<sup>4</sup> C. Brown,<sup>5</sup> T. Brunner,<sup>1,6</sup> J. D. Cardona,<sup>1,7</sup> D. Curien,<sup>8</sup> I. Dedes,<sup>9</sup> T. Dickel,<sup>4,10</sup> J. Dudek,<sup>8,11</sup> E. Dunling,<sup>1,12</sup> G. Gwinner,<sup>7</sup> Z. Hockenbery,<sup>1,6</sup> J. D. Holt,<sup>1,13</sup> C. Hornung,<sup>10</sup> C. Izzo,<sup>1</sup> A. Jacobs,<sup>1,2</sup> A. Javaji,<sup>1,2</sup> B. Kootte,<sup>1,7</sup> G. Kripkó-Koncz,<sup>4</sup> E. M. Lykiardopoulou,<sup>1,2</sup> T. Miyagi,<sup>1</sup> I. Mukul,<sup>1</sup> T. Murböck,<sup>1</sup> W. R. Plaß,<sup>4,10</sup> M. P. Reiter,<sup>1,4,5</sup> J. Ringuette,<sup>1,14</sup> C. Scheidenberger,<sup>4,10,15</sup> R. Silwal,<sup>1,†</sup> C. Walls,<sup>1,7</sup> H. L. Wang,<sup>16</sup> Y. Wang,<sup>1,2</sup> J. Yang,<sup>11,16</sup> J. Dilling,<sup>1,2</sup> and A. A. Kwiatkowski<sup>1,17</sup>

<sup>1</sup>TRIUMF, 4004 Wesbrook Mall, Vancouver, British Columbia V6T 2A3, Canada

<sup>2</sup>Department of Physics & Astronomy, University of British Columbia, Vancouver, British Columbia V6T 1Z1, Canada

<sup>3</sup>Department of Physics & Astronomy, University of Calgary, Calgary, Alberta T2N 1N4, Canada

<sup>4</sup>II. Physikalisches Institut, Justus-Liebig-Universität, 35392 Gießen, Germany

<sup>5</sup>School of Physics and Astronomy, University of Edinburgh, Edinburgh, EH9 3FD, United Kingdom

<sup>6</sup>Department of Physics, McGill University, 3600 Rue University, Montréal, QC H3A 2T8, Canada

<sup>7</sup>Department of Physics & Astronomy, University of Manitoba, Winnipeg, Manitoba R3T 2N2, Canada

<sup>8</sup>Université de Strasbourg, CNRS, IPHC UMR 7178, F-67 037 Strasbourg, France

<sup>9</sup>Institute of Nuclear Physics, Polish Academy of Sciences, PL-31 342 Kraków, Poland

<sup>10</sup>GSI Helmholtzzentrum für Schwerionenforschung GmbH, Planckstraße 1, 64291 Darmstadt, Germany

<sup>11</sup>Institute of Physics, Marie Curie-Skłodowska University, PL-20 031 Lublin, Poland

<sup>12</sup>Department of Physics, University of York, York, YO10 5DD, United Kingdom

<sup>13</sup>Department of Physics, McGill University, Montréal, QC H3A 2T8, Canada

<sup>14</sup>Department of Physics, Colorado School of Mines, Golden, Colorado 80401, USA

<sup>15</sup>Helmholtz Forschungsakademie Hessen für FAIR (HFHF), GSI Helmholtzzentrum für Schwerionenforschung, Campus Gießen, 35392 Gießen, Germany

<sup>16</sup>School of Physics and Microelectronics, Zhengzhou University, Zhengzhou 4500001, China

<sup>17</sup>Department of Physics and Astronomy, University of Victoria, Victoria, British Columbia V8P 5C2, Canada



(Received 19 July 2021; revised 24 December 2021; accepted 16 March 2022; published 19 April 2022)

Nuclear properties across the chart of nuclides are key to improving and validating our understanding of the strong interaction in nuclear physics. We present high-precision mass measurements of neutron-rich Fe isotopes performed at the TITAN facility. The multiple-reflection time-of-flight mass spectrometer (MR-ToF-MS), achieving a resolving power greater than 600 000 for the first time, enabled the measurement of  $^{63-70}\text{Fe}$ , including first-time high-precision direct measurements ( $\delta m/m \approx 10^{-7}$ ) of  $^{68-70}\text{Fe}$ , as well as the discovery of a long-lived isomeric state in  $^{69}\text{Fe}$ . These measurements are accompanied by both mean-field and *ab initio* calculations using the most recent realizations which enable theoretical assignment of the spin-parities of the  $^{69}\text{Fe}$  ground and isomeric states. Together with mean-field calculations of quadrupole deformation parameters for the Fe isotope chain, these results benchmark a maximum of deformation in the  $N = 40$  island of inversion in Fe and shed light on trends in level densities indicated in the newly refined mass surface.

DOI: [10.1103/PhysRevC.105.L041301](https://doi.org/10.1103/PhysRevC.105.L041301)

The evolution of nuclear structure away from stability is a primary focus of low-energy nuclear physics. This concerns the change in nuclear stability with proton number  $Z$  and/or neutron number  $N$ , departing from the spherical-shape (“magic”) shell-closures at 2, 8, 20, 28, 50, 82, and 126. Among the most powerful theoretical approaches are the nuclear mean-field and the spherical shell model. Underlying the magic spherical shell closures, we find the single-nucleon energy levels with an ordering, as shown, e.g., in Fig. 4.4 of

Ref. [1]. For orbitals between  $Z = 20$  and  $Z = 50$ , we find the following order:  $1f_{7/2}$ ,  $2p_{3/2}$ ,  $1f_{5/2}$ ,  $2p_{1/2}$ , and  $1g_{9/2}$ .

Within this terminology, certain variations in the energies of the above order are called inversions. Groups of nuclei for which such a different order applies are referred to as *islands of inversion*; they are often signaled by an approaching of levels as functions of  $Z$  and/or  $N$ , permitting increased neutron or proton excitations associated with islands of inversion [2].

When filling orbitals in between spherical shell closures, we enter an increased level-density zone with shell-energies privileging nonzero quadrupole deformation, a natural degree of freedom in the mean-field approach. Within the spherical shell model, one expresses the same via an increase of the  $B(E2)$ , and/or lowering the first-excited  $I^\pi = 2^+$

\*wporter@triumf.ca

<sup>†</sup>Present address: Department of Physics and Astronomy, Appalachian State University, Boone, North Carolina 28608, USA.

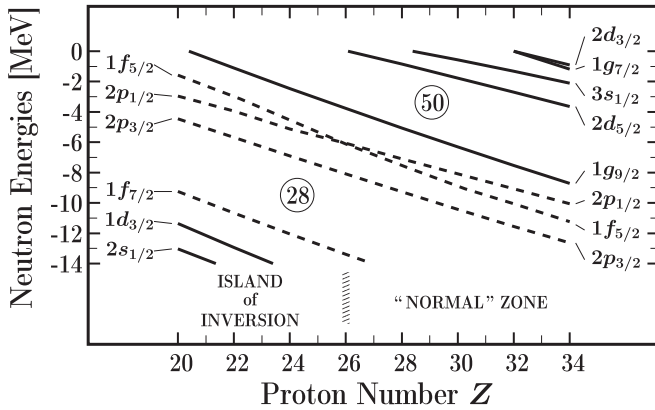


FIG. 1. Neutron energies based on the Universal Woods-Saxon Hamiltonian from Ref. [7] along  $N = 40$  for spherical shape nuclei; solid (dashed) lines stand for positive-parity (negative-parity) orbitals. The close approach of orbitals  $2p_{1/2}$  and  $1f_{5/2}$  at  $Z = 26$  defines a zone of nuclei usually referred to as an “island of inversion.”

energies. Both can be seen as differing language for the same physics content of mean-field deformation. The region around  $N = 40$  has gained interest due to the presence of such phenomena [3–6] as potential indicators of deformation and inversion.

To examine the single-neutron spectrum in the vicinity of  $N = 40$ , we have calculated single-particle energies, as shown in Fig. 1. Here we follow the state-of-the-art phenomenological realization of the universal mean-field approach [7], where one set of parameters is common for the whole nuclear chart, parametric correlations of the modeling are analyzed and removed according to the mathematical inverse problem theory. The approach of the  $2p_{1/2}$  and  $1f_{5/2}$  levels at  $Z = 26$  impacts the ground-state structures of nuclei in the two zones, “inversion” and “normal,” in different manners, highlighted by the structure differences of the two-body matrix elements of the residual interactions, collective excitation energies, and decay strengths. This region has been termed  $N = 40$  *island of inversion* in the shell-model literature.

Experiments in this neutron-rich  $Z = 24$ – $28$  region have been challenging, in large part due to elemental production difficulties. ISOL-type facilities have historically not been considered viable options for the production of transition metals [8,9].

Despite experimental challenges, many measurements have played a role in probing the nuclear structure of this region [10,11]. Large  $B(E2; 0^+ \rightarrow 2^+)$  [12], increasing charge radii [13], and increasing  $E(4^+)/E(2^+)$  ratios [14] have all been interpreted as stemming from the presence of deformed nuclei due to neutron excitations into intruding orbitals, indicative of an island of inversion. On the mass-measurement front, previous studies show a flattening behavior in the two-neutron separation energies along the Cr and Mn isotopes [6,15]. This is often interpreted as indicative of increasing deformation. For the Fe isotopes, although data on masses are available, precisions pale in comparison to neighboring isotope chains in the region. Current low-resolution experimental data suggest maximum collectivity is reached at  $N =$

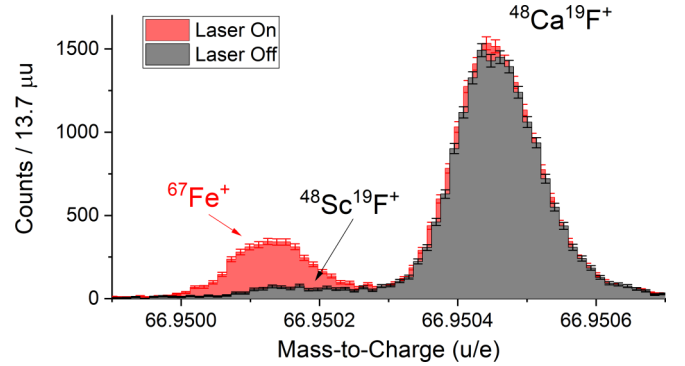


FIG. 2. A portion of the mass spectra at  $A = 67$  with TRILIS lasers on and off. A factor 4.5 count increase in the leftmost peak with lasers unambiguously confirms its identity as  $^{67}\text{Fe}$ .

42 [16], but greater precisions are needed to make definitive conclusions.

In this article, we present precision mass measurements of  $^{63-70}\text{Fe}$  from the TITAN Multiple-Reflection Time-of-Flight Mass Spectrometer (MR-ToF-MS) [17], including the first high-precision ( $\delta m/m \approx 10^{-7}$ ) direct measurements of  $^{68-70}\text{Fe}$ . This represents the first large-scale investigation of such neutron-rich Fe at an ISOL facility, supported by resonant laser ion source development. These results are interpreted in terms of mean-field calculations employing recent “universal” Woods-Saxon Hamiltonian [7] and results from the newly developed multishell valence-space in-medium similarity renormalization group (VS-IMSRG) [18].

Fe mass measurements were performed at TRIUMF’s Ion Trap for Atomic and Nuclear science (TITAN) [19]. Fe isotopes were produced at TRIUMF’s Isotope Separator and Accelerator (ISAC) [20], where a 480 MeV, 20  $\mu\text{A}$  proton beam was impinging on a  $\text{UCX}$  target. Reaction products were surface ionized by a hot Re ion source. Further ionization of Fe isotopes was achieved via TRIUMF’s resonant ionization laser ion source (TRILIS), using a two-step resonant laser excitation scheme [21]. This Fe-specific scheme, used here for the first time, allowed for increased yields by at least two to three orders of magnitude of Fe ions of interest and confirmed the presence of Fe species in spectra, as seen in Fig. 2.

Ionized beams were sent to a mass separator ( $R = 2000$ ) which removed nonisobaric products. The isobaric beam was then transported to the TITAN facility, where it was cooled and bunched via the TITAN radio-frequency quadrupole (RFQ) cooler and buncher [22]. Cooled ion bunches were sent to the TITAN MR-ToF-MS [17] for mass measurement.

The MR-ToF-MS determines the masses of ions via their time-of-flight over a given path and kinetic energy [23–25]. After cooling and injection in the system, bunches underwent between 974 to 1008 isochronous turns between electrostatic mirrors for a total time-of-flight of  $\approx 16$  ms before ejection onto a MagneToF detector [26] for time-of-flight detection. To measure and detect masses of very low signal-to-background ratios ( $< 1$  to  $10^{-4}$ ), mass-selective re trapping was employed [27–29].

Overall, the measurement process ran with a cycle time of  $\approx 33$  ms, yielding mass resolutions of  $R > 600\,000$ , the

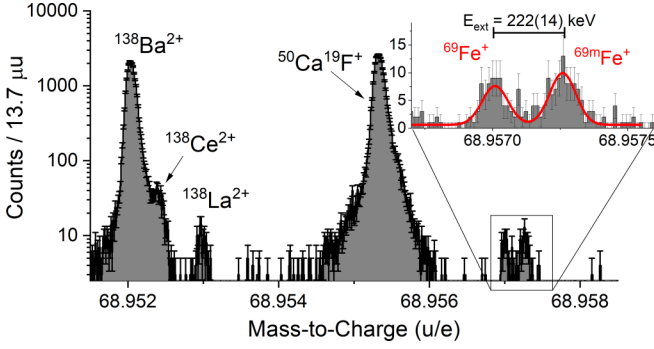


FIG. 3. A portion of the mass spectra at  $A = 69$ . The identified mass species are labeled. In the inset,  $^{69}\text{Fe}$  and the newly discovered  $^{69m}\text{Fe}$  are shown

highest achieved with the TITAN MR-ToF-MS. This high resolving power allowed for separation of a  $\approx 200$  keV isomeric state in  $^{69}\text{Fe}$  as shown in Fig. 3.

Time-of-flight spectra were converted to mass spectra via the relationship  $m_{\text{ion}}/q = C(t_{\text{ion}} - t_0)^2$ , where  $t_0$  is  $0.16 \mu\text{s}$  as determined offline and  $C$  is a calibration factor determined from a high-statistics, well-known reference ion in each spectrum, as listed in Table I. To account for time-dependent drifts, a time-resolved calibration (TRC) was performed [30] using the mass data-acquisition software package [31]. Peak centroids were determined by fitting hyper-EMG functions [32] using the EMGFIT Python wrapper [33]. Statistical uncertainties are generated based on techniques described in Refs. [30,33]. Systematic uncertainties of the MR-ToF-MS system are described in detail in Refs. [30,34], and total to a value of  $\approx 8.6 \times 10^{-8}$ . This uncertainty is dominated by the uncertainties due to ion-ion interactions ( $3.3 \times 10^{-8}$  per detected ion), TRCs ( $\approx 3.7 \times 10^{-8}$ ), and the nonideal switching of mirrors ( $7.0 \times 10^{-8}$ ). For  $^{67}\text{Fe}$ , the presence of underlying counts of  $^{48}\text{Sc}^{19}\text{F}$  had to be considered, as shown in Fig. 2. Therefore, an uncertainty of 6.7 keV was added in quadrature, following the prescription in Ref. [30] for the treatment of overlapping peaks. In the case of  $^{70}\text{Fe}$ , where a doubly charged reference ion was used, an uncertainty of 3.8 keV was

added in quadrature to account for differences in peak shape between singly and doubly charged ions.

Table I reports the masses of all measured Fe isotopes, as well their mass excesses as found in literature. The masses of  $^{63-66}\text{Fe}$  have been well established, and our experimental results are in agreement ( $< 0.6\sigma$ ) with these values.  $^{68,69,70}\text{Fe}$  constitute the first direct mass measurements with precisions of  $\delta m/m \approx 10^{-7}$ , with previous measurements done via TOF-B $\rho$  mass spectrometry [16]. The case of  $^{67}\text{Fe}$  is notable, as our results deviate from a recent Penning trap mass measurement at JYFLTRAP [35] by  $\approx 32\sigma$ . As seen in Fig. 2, our identification of  $^{67}\text{Fe}$  is confirmed with the species-specific resonant laser excitation scheme via a factor 4.5 count increase of the Fe peak. The mass value reported by Ref. [35] coincides with the  $^{48}\text{Ca}^{19}\text{F}$  peak, which showed no statistically significant count change with lasers. Given the expected count increase of Fe species with lasers, our data do not indicate the presence of a long-lived isomer in  $^{67}\text{Fe}$ , which is unexpected given their presence in the other odd-even Fe isotopes. In both experiments, the known 387 keV isomeric state in  $^{67}\text{Fe}$  is too short lived ( $t_{1/2} = 75 \mu\text{s}$ ) to have been measured with the techniques used.

Alongside high-precision ground-state mass measurements, a long-lived isomeric state in  $^{69}\text{Fe}$  was discovered and evaluated with an excitation energy of  $E_x = 222(14)$  keV, see Fig. 3. This identification is strengthened by the observation of the well-known isomeric state in  $^{65m}\text{Fe}$ , whose excitation energy was determined to be  $E_x = 397(11)$  keV, in excellent agreement with the literature [37]. This represents another odd-even isomer in the Fe isotope chain. To estimate the half-life of the new isomeric state, a storage time measurement was performed, similar to Ref. [38], which suggests a half-life on the order of 100–200 ms. The detected isomer–ground-state pairs for  $^{65}\text{Fe}$  and  $^{69}\text{Fe}$  had isomer-to-ground count ratios of 3.31(3) and 1.33(17), respectively. It is not possible to deduce the structure of  $^{69}\text{Fe}$  states from our experiment since the spin-parity assignments are not known. We propose an interpretation based on mean-field calculations and the properties of the sequence of  $^{63-69}\text{Fe}$  isomers, where experimental spin-parity assignments remain inconclusive past  $^{65}\text{Fe}$ .

TABLE I. Results of the mass measurements performed, compared with the values recommended by AME2020 [36] for  $^{63-67}\text{Fe}$  and values from [16] for  $^{68-70}\text{Fe}$ . Values with a superscript  $D$  are unused in the mass calculation in Ref. [36]. We also provide the mass ratio ( $m_{\text{ionic,IOI}}/m_{\text{ionic,ref}}$ ) between the ionic masses of the ion of interest (IOI) and the reference ion. All mass values are in keV. All Fe isotopes were measured as singly charged ions. Uncertainties presented are total uncertainties calculated as  $\sigma_{\text{total}} = (\sigma_{\text{sys}}^2 + \sigma_{\text{stat}}^2)^{1/2}$ .

Nuclide	Mass excess	Literature	Difference	Reference ion	Mass ratio
$^{63}\text{Fe}$	−55635.4(5.4)	−55635.6(4.3)	−0.3 (6.9)	$^{44}\text{Ca}^{19}\text{F}^+$	0.999 792 4940 (931)
$^{64}\text{Fe}$	−54970.0(5.3)	−54969.6(5.0)	0.5 (7.3)	$^{48}\text{Ti}^{16}\text{O}^+$	0.999 979 3643 (887)
$^{65}\text{Fe}$	−51218.7(8.4)	−51217.9(5.1)	0.8 (9.8)	$^{46}\text{Ti}^{19}\text{F}^+$	0.999 915 835 (144)
$^{65m}\text{Fe}$	−50821.4(7.7)	−50823.9(7.2)	−2.5(10.5)	$^{46}\text{Ti}^{19}\text{F}^+$	0.999 922 402 (133)
$^{66}\text{Fe}$	−50061 (10)	−50067.8(4.1)	−6.9(11.0)	$^{50}\text{Ti}^{16}\text{O}^+$	1.000 107 763 (165)
$^{67}\text{Fe}$	−46014.8(8.7)	−45708.4(3.8)	306.3(9.5)	$^{48}\text{Ti}^{19}\text{F}^+$	1.000 071 788 (140)
$^{68}\text{Fe}$	−44100.9(5.6)	−44360(320) <sup>D</sup>	−259 (320)	$^{68}\text{Ga}^+$	1.000 371 3423 (916)
$^{69}\text{Fe}$	−39504 (11)	−40270(400) <sup>D</sup>	−767 (400)	$^{50}\text{Ti}^{19}\text{F}^+$	1.000 216 864 (164)
$^{69m}\text{Fe}$	−39281.7(9.1)			$^{50}\text{Ti}^{19}\text{F}^+$	1.000 220 318 (142)
$^{70}\text{Fe}$	−37053 (12)	−37710(490) <sup>D</sup>	−657 (490)	$^{140}\text{Ba}^{2+}$	1.000 085 987 (213)

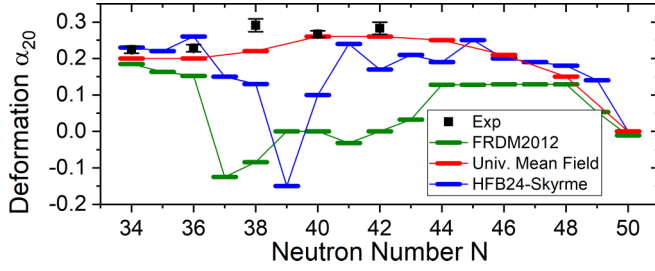


FIG. 4. Experimental quadrupole deformation for Fe isotopes from Ref. [39] in comparison with theoretical calculations.

Figure 1 shows the transition into the  $N = 40$  island of inversion, seen, for example, in the approaching of the  $2p_{1/2}$  and  $1f_{5/2}$  levels in spherical nuclei. However, known equilibrium shapes across  $N = 40$  [39] are all nonspherical and manifest systematically prolate shapes, which will further shift the corresponding energy levels. We performed large-scale mean-field calculations, employing the “universal” Woods-Saxon Hamiltonian [7], and extracted deformation and single-particle energy levels. Our calculations are in good agreement with known experimental deformations across  $N = 40$  and predict a return to sphericity approaching  $N = 50$ , as shown in Fig. 4. The trends at  $N = 40$  deviate from FRDM [40] and HFB [41] calculations. In Fig. 5 we show the single-particle neutron energies for different quadrupole deformations  $\alpha_{20}$ .

In  $^{65}\text{Fe}$ , the experimental  $I_{\text{g.s.}}^{\pi} = (1/2^-)$  [37] corresponds to the 39th neutron occupying the  $p_{1/2}$  orbital very close to the  $N = 40$  gap at  $\alpha_{20} \approx 0.20$ , as in Fig. 5. The  $I_{\text{i.s.}}^{\pi} = (9/2^+)$  isomer at 402 keV corresponds to the first-excited orbital  $g_{9/2}$ , and the nearby  $I_{\text{i.s.}}^{\pi} = (5/2^-)$  at 397 keV corresponds to  $f_{5/2}$ .

Experimentally, the 41st neutron in  $^{67}\text{Fe}$  has an uncertain spin-parity assignment, either  $5/2^+$  or  $7/2^+$  [37], in conflict with  $I_{\text{g.s.}}^{\pi} = 1/2^-$  together with  $5/2^-$  at 366.4 keV proposed in Ref. [42]. The latter assignments are in good qualitative

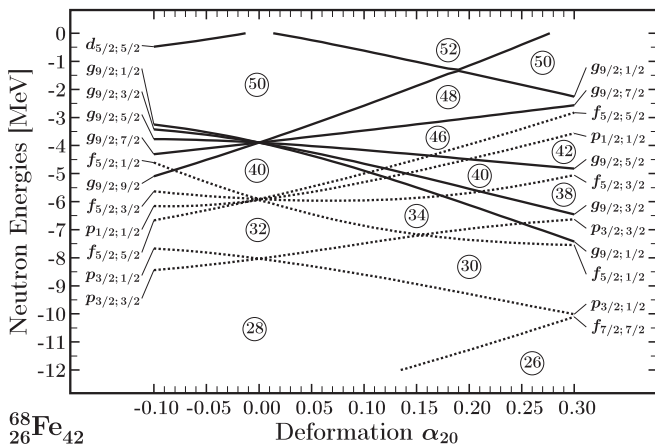


FIG. 5. Mean-field single-particle neutron energies obtained with the Woods-Saxon Hamiltonian from Ref. [7], showing neutron orbital patterns in  $^{63-69}\text{Fe}$  nuclei. Note that  $p_{1/2}$  and  $f_{5/2}$  orbitals, placed between  $N = 32$  and  $N = 40$  occupations, are nearly degenerate at  $\alpha_{20} \approx 0$ .

correspondence with the closeness of  $p_{1/2}$  and  $f_{5/2}$  orbitals at  $\alpha_{20} \approx 0.20$ .

According to our calculations,  $^{68}\text{Fe}$  and  $^{70}\text{Fe}$  are strongly quadrupole deformed, in agreement with the experimental value  $\alpha_{20} = 0.283$  for  $^{68}\text{Fe}$  [39]. From the perspective in Fig. 5, at  $\alpha_{20}$  exceeding 0.20, the 43rd neutron in  $^{69}\text{Fe}$  occupies the  $p_{1/2}$  orbital, with the closely lying  $f_{5/2}$  and  $g_{9/2}$  orbitals giving rise to the  $I^{\pi} = 5/2^-$  and  $9/2^+$  excited states. Assuming decays are via  $\gamma$  deexcitations given global isomeric properties [43] and preexisting data in the Fe chain [37], the isomeric candidate  $I_{\text{i.s.}}^{\pi} = 9/2^+$  would decay via an  $M4$  transition, whereas the  $5/2^-$  could decay via an  $E2$  transition. Given  $E_{\gamma} = 222$  keV, our elementary Weisskopf modeling indicates the  $M4$  decay is most likely for a long-lived isomer given the Woods-Saxon diagram expectations and our measured half-life. Thus a tentative spin assignment of  $I_{\text{i.s.}}^{\pi} = 9/2^+$  is favored.

To confirm our spin-parity assignment methodology, we checked the  $N = 41$ st nucleon configuration in  $^{69}\text{Ni}$ , taking into account that, according to our calculations,  $^{68}\text{Ni}$  and  $^{70}\text{Ni}$  are almost spherical. At small deformation,  $\alpha_{20} < 0.1$ , the 41st neutron occupies the  $g_{9/2}$  orbital; experimentally,  $I_{\text{g.s.}}^{\pi} = 9/2^+$  is in agreement with our arguments. The lowest-lying excited states have  $I^{\pi} = 1/2^-$  and  $5/2^-$ , again compatible with the near degeneracy of the  $p_{1/2}$  and  $f_{5/2}$  orbitals in Fig. 5.

Figure 6 shows the two-neutron separation energies ( $S_{2n}$ ) for the  $Z = 24-28$  isotopes, defined as  $S_{2n}(N, Z) = m(N-2, Z) + 2m_n - m(N, Z)$ , with  $m(N, Z)$  being the mass excess and  $m_n$  being the mass of the neutron. Our results show an upward curvature in the  $S_{2n}$  trend in the Fe isotope chain up until  $N = 41$ . Also shown is  $\delta_{2n}^*$ , given as  $\delta_{2n}^* = S_{2n}(N-2, Z) - S_{2n}(N, Z)$ . As a pseudoderivative of  $S_{2n}$ , low- $\delta_{2n}^*$  values decreasing towards zero indicate a flattening in  $S_{2n}$ , whereas a sharp peak indicates a steep drop-off in  $S_{2n}$  at  $N-2$ . Such sharp peaks, when at even neutron numbers, are typically indicative of bigger energy-level gaps [44]. The local maximum at  $N = 43$ , as opposed to  $N = 42$ , therefore indicates the absence of a large level gap for Fe at  $N = 40$ . The neutron pairing gap  $P_n$  is also shown, given as  $P_n(N, Z) = (-1)^N [B(N+1, Z) + B(N-1, Z) - 2B(N, Z)]/2$ , where  $B(N, Z)$  is the binding energy for which we use a positive sign convention. Our high-precision results show a smooth reduction in the odd-even staggering of the pairing gap as  $N = 42$  is approached, in contrast with previous results from Refs. [35] and [16].

To further interpret the refined mass surface around  $N = 40$ , we compare the trends with trends in deformations in the Fe isotope chain, shown in Fig. 4. Our calculations predict the onset of quadrupole equilibrium deformations beginning at  $^{60}\text{Fe}$  with  $\alpha_{20} = 0.20$ , followed by  $\alpha_{20} = 0.20, 0.22, 0.26, 0.26, 0.25$ , and  $0.21$  for  $^{62, 64, 66, 68, 70, 72}\text{Fe}$ , respectively. The maximum quadrupole deformation occurs between  $^{66}\text{Fe}$  and  $^{68}\text{Fe}$  (i.e.,  $N = 40$  and  $N = 42$ ). This corresponds to the  $\delta_{2n}^*$  minimum at  $N = 41$ , indicating the maximum level density, and therefore maximum deformation, is correlated to the minimum change in  $S_{2n}$ . These results reveal the deformation maximum point in the Fe isotope chain. In comparison, here the FRDM [40] and HFB [41] calculations follow the refined  $S_{2n}$  trend with only small fluctuations,



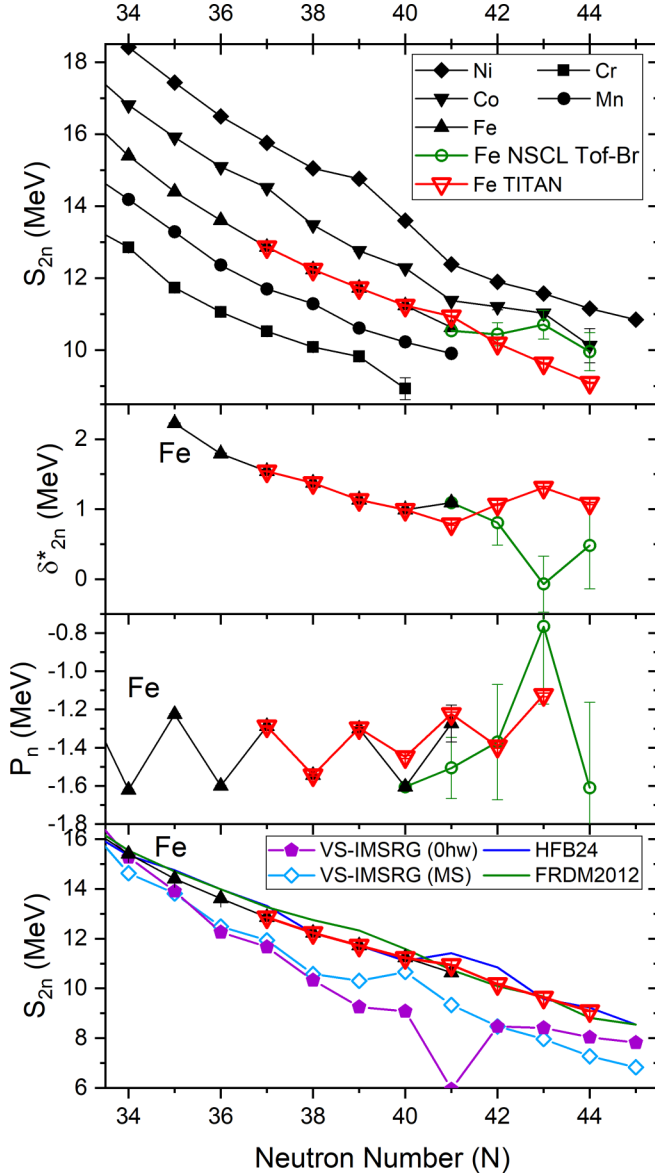


FIG. 6. (top) A graph of the  $S_{2n}$  in the  $Z = 24$ – $28$  isotope chains based on mass values from Refs. [36] and [16], and  $^{63-70}\text{Fe}$  mass measurements from this work. Of note, the new high-precision TITAN measurements reach as far as the previous ToF-B $\rho$  results from Ref. [16]. (middle top) A graph of the  $\delta_{2n}^*$  for the Fe isotope chain showing a minimum at  $N = 41$ . (middle bottom) A graph of the pairing gap  $P_n$  from three-point binding-energy differences for the Fe isotopes. (bottom) A graph of Fe  $S_{2n}$  experimental values compared with theoretical calculations for VS-IMSRG results from Ref. [45] ( $0\hbar\omega$ ) and this work (MS). The discrepant points at  $N = 40$  (MS) and  $N = 41$  ( $0\hbar\omega$ ) are shown for completeness, despite the fact they are artifacts of mismatched neutron valence spaces.

despite predicting nearly spherical shapes for the Fe nuclei across  $N = 40$ .

To examine the results within a different theoretical framework, we present *ab initio* predictions using VS-IMSRG [46–48] calculations. We use the 1.8/2.0(EM) NN + 3N interaction [49,50], which globally predicts ground-state

energies at least to the  $^{132}\text{Sn}$  region [45,51,52]. In particular, separation energies below and above the  $N = 40$  island of inversion region [15,44,53,54] have generally been well reproduced. Following the  $0\hbar\omega$  approach in Ref. [45], we take a  $pf$  and  $sdg$  neutron valence space below and above  $N = 40$ , respectively. This method, however, makes predictions across  $N = 40$  difficult. To obtain a more reliable description across the  $N = 40$  gap, we employ the newly developed multishell (MS) approach [18], where we take a neutron  $p_{1/2}$ ,  $p_{3/2}$ ,  $f_{5/2}$ ,  $g_{9/2}$  space above a  $^{48}\text{Ca}$  core. The resulting valence-space Hamiltonians were diagonalized with the KSHELL code [55].  $S_{2n}$  values from the two prescriptions are shown in Fig. 6.

Both methods show an offset compared with the experimental  $S_{2n}$  beyond  $N > 35$ , also observed in Cr [15]. The behavior is a consequence of the negligence of many-body correlations beyond the VS-IMSRG(2) approximation [47] and implies an enhancement in collectivity beyond  $N > 35$ , in agreement with our mean-field calculations. The discrepant point at  $N = 40$  ( $N = 41$  for the  $0\hbar\omega$  calculations) is an artifact of continuations due to remaining mismatched  $pf$  and  $sdg$  neutron valence spaces. Nonetheless, the MS values display trends similar to the experimental mass surface. Although there is still a deviation between our experimental results and the MS calculations, significant improvement is shown over the previous  $0\hbar\omega$  VS-IMSRG calculation method. This paves the way towards a complete *ab initio* picture of the  $N = 40$  island of inversion.

In conclusion, we have presented the measurements of neutron-rich Fe isotopes performed at the TITAN facility using its MR-ToF-MS. These results represent a significant increase in precision for three first-time direct mass measurements of a precision  $\approx 10^{-7}$  and include the discovery of a new long-lived odd-even isomer, accomplished with the first-time use of Fe beams at an ISOL facility. The pairing of the highly efficient TITAN MR-ToF-MS system with an Fe specific laser ionization scheme enabled the reach of exotic Fe isotopes comparable to that of the NSCL ToF-B $\rho$  measurements, paving the way for future high-precision mass campaigns. These measurements, together with the pairing of coherent interpretations employing state-of-the-art mean-field and *ab initio* calculations, refine our understanding of nuclear structure around the  $N = 40$  island of inversion and establish a deformation maximum point in the Fe isotope chain. Further spectroscopic data are needed to experimentally determine the spin of the newly discovered  $^{69}\text{Fe}$  isomer. Nonetheless, the connection of the mass surface to nuclear deformation showcases the importance of nuclear masses in the search for deformation across all regions of the nuclear chart. In particular, more neutron-rich precision mass measurements in the  $Z = 24$ – $28$  region are needed to resolve nuclear structure effects as  $N = 50$  is approached.

The authors would like to thank S.R. Stroberg for the IMSRG++ code [56] used to perform VS-IMSRG calculations and J. Lassen and the laser ion source group at TRIUMF for their development of the Fe laser scheme. This work was supported by the Natural Sciences and Engineering Research Council (NSERC) of Canada under Grants No. SAPIN-2018-00027 and No. RGPAS-2018-522453, and by the

National Research Council (NRC) of Canada through TRIUMF, the Polish National Science Centre under Contract No. 2016/21/B/ST2/01227, the Polish-French COPIN-IN2P3 collaboration agreement under project numbers 04-113 and 05-119 and COPIGAL 2020, the UKRI Science and Technology Facilities Council (STFC) Grant No. ST/P004008/1, the U.S. Department of Energy, Office of Science, Office of Nuclear Physics under Grant No. DE-FG02-93ER40789, and the German Research Foundation (DFG), Grant No. SCHE 1969/2-1, by the German Federal Ministry for Education and Research (BMBF), Grant No. 05P19RGFN1 and

05P21RGFN1, by the Hessian Ministry for Science and Art through the LOEWE Center HICforFAIR, by the JLU and GSI under the JLU-GSI strategic Helmholtz partnership agreement. Support from the National Natural Science Foundation of China, Grant No. 11975209, and the Physics Research and Development Program of Zhengzhou University, Grant No. 32410017 is acknowledged. Computations were performed with an allocation of computing resources on Cedar at WestGrid and Compute Canada, and on the Oak Cluster at TRIUMF managed by the University of British Columbia department of Advanced Research Computing (ARC).

- [1] W. Hornyak, *Nuclear Structure* (Academic Press, Cambridge, MA, 1975).
- [2] J. Ljungvall, A. Görgen, A. Obertelli, W. Korten, E. Clément, G. de France, A. Bürger, J.-P. Delaroche, A. Dewald, A. Gadea, L. Gaudefroy, M. Girod, M. Hackstein, J. Libert, D. Mengoni, F. Nowacki, T. Pissulla, A. Poves, F. Recchia, M. Rejmund *et al.*, Onset of collectivity in neutron-rich Fe isotopes: Toward a new island of inversion? *Phys. Rev. C* **81**, 061301(R) (2010).
- [3] M. Hannawald, T. Kautzsch, A. Wöhr, W. B. Walters, K.-L. Kratz, V. N. Fedoseyev, V. I. Mishin, W. Böhmer, B. Pfeiffer, V. Sebastian, Y. Jading, U. Köster, J. Lettry, H. L. Ravn, and the ISOLDE Collaboration, Decay of Neutron-Rich Mn Nuclides and Deformation of Heavy Fe Isotopes, *Phys. Rev. Lett.* **82**, 1391 (1999).
- [4] O. Sorlin, C. Donzaud, F. Nowacki, J. C. Angélique, F. Azaiez, C. Bourgeois, V. Chisté, Z. Dlouhy, S. Grévy, D. Guillemaud-Mueller, F. Ibrahim, K.-L. Kratz, M. Lewitowicz, S. M. Lukyanov, J. Mrasek, Y.-E. Penionzhkevich, F. de Oliveira Santos, B. Pfeiffer, F. Pougheon, A. Poves *et al.*, New region of deformation in the neutron-rich  $^{60}\text{Cr}_{36}$  and  $^{62}\text{Cr}_{38}$ , *Eur. Phys. J. A* **16**, 55 (2003).
- [5] A. Gade, R. V. F. Janssens, T. Baugher, D. Bazin, B. A. Brown, M. P. Carpenter, C. J. Chiara, A. N. Deacon, S. J. Freeman, G. F. Grinyer, C. R. Hoffman, B. P. Kay, F. G. Kondev, T. Lauritsen, S. McDaniel, K. Meierbachtol, A. Ratkiewicz, S. R. Stroberg, K. A. Walsh, D. Weisshaar *et al.*, Collectivity at  $N = 40$  in neutron-rich  $^{64}\text{Cr}$ , *Phys. Rev. C* **81**, 051304(R) (2010).
- [6] S. Naimi, G. Audi, D. Beck, K. Blaum, C. Böhm, C. Borgmann, M. Breitenfeldt, S. George, F. Herfurth, A. Herlert, A. Kellerbauer, M. Kowalska, D. Lunney, E. Minaya Ramirez, D. Neidherr, M. Rosenbusch, L. Schweikhard, R. N. Wolf, and K. Zuber, Surveying the  $N = 40$  island of inversion with new manganese masses, *Phys. Rev. C* **86**, 014325 (2012).
- [7] A. Gaamouci, I. Dedes, J. Dudek, A. Baran, N. Benhamouda, D. Curien, H. L. Wang, and J. Yang, Exotic toroidal and superdeformed configurations in light atomic nuclei: Predictions using a mean-field Hamiltonian without parametric correlations, *Phys. Rev. C* **103**, 054311 (2021).
- [8] R. Kirchner, K. Burkard, W. Hüller, and O. Klepper, Ion source development for the on-line isotope separator at GSI, *Nucl. Instrum. Methods Phys. Res., Sect. B* **70**, 56 (1992).
- [9] U. Köster, P. Carbonez, A. Dorsival, J. Dvorak, R. Eichler, S. Fernandes, H. Frånberg, J. Neuhausen, Z. Novackova, R. Wilfinger, and A. Yakushev, (Im-)possible ISOL beams, *Eur. Phys. J. Spec. Top.* **150**, 285 (2007).
- [10] M. Block, C. Bachelet, G. Bollen, M. Facina, C. M. Folden, C. Guénaut, A. A. Kwiatkowski, D. J. Morrissey, G. K. Pang, A. Prinke, R. Ringle, J. Savory, P. Schury, and S. Schwarz, Discovery of a Nuclear Isomer in  $^{65}\text{Fe}$  with Penning Trap Mass Spectrometry, *Phys. Rev. Lett.* **100**, 132501 (2008).
- [11] R. Ferrer, M. Block, C. Bachelet, B. R. Barquest, G. Bollen, C. M. Campbell, M. Facina, C. M. Folden, C. Guénaut, A. A. Kwiatkowski, D. L. Lincoln, D. J. Morrissey, G. K. Pang, A. M. Prinke, R. Ringle, J. Savory, P. Schury, and S. Schwarz, Penning trap mass spectrometry of neutron-rich Fe and Co isotopes around  $N = 40$  with the LEBIT mass spectrometer, *Phys. Rev. C* **81**, 044318 (2010).
- [12] W. Rother, A. Dewald, H. Iwasaki, S. M. Lenzi, K. Starosta, D. Bazin, T. Baugher, B. A. Brown, H. L. Crawford, C. Fransen, A. Gade, T. N. Ginter, T. Glasmacher, G. F. Grinyer, M. Hackstein, G. Ilie, J. Jolie, S. McDaniel, D. Miller, P. Petkov *et al.*, Enhanced Quadrupole Collectivity at  $N = 40$ : the Case of Neutron-Rich Fe Isotopes, *Phys. Rev. Lett.* **106**, 022502 (2011).
- [13] H. Heylen, C. Babcock, R. Beerwerth, J. Billowes, M. L. Bissell, K. Blaum, J. Bonnard, P. Campbell, B. Cheal, T. Day Goodacre, D. Fedorov, S. Fritzsche, R. F. Garcia Ruiz, W. Geithner, C. Geppert, W. Gins, L. K. Grob, M. Kowalska, K. Kreim, S. M. Lenzi *et al.*, Changes in nuclear structure along the Mn isotopic chain studied via charge radii, *Phys. Rev. C* **94**, 054321 (2016).
- [14] C. Santamaria, C. Louchart, A. Obertelli, V. Werner, P. Doornenbal, F. Nowacki, G. Authalet, H. Baba, D. Calvet, F. Château, A. Corsi, A. Delbart, J.-M. Gheller, A. Gillibert, T. Isobe, V. Lapoux, M. Matsushita, S. Momiyama, T. Motobayashi, M. Niikura *et al.*, Extension of the  $N = 40$  Island of Inversion Towards  $N = 50$ : Spectroscopy of  $^{66}\text{Cr}$ ,  $^{70,72}\text{Fe}$ , *Phys. Rev. Lett.* **115**, 192501 (2015).
- [15] M. Mougéot, D. Atanasov, K. Blaum, K. Chrysalidis, T. D. Goodacre, D. Fedorov, V. Fedosseev, S. George, F. Herfurth, J. D. Holt, D. Lunney, V. Manea, B. Marsh, D. Neidherr, M. Rosenbusch, S. Rothe, L. Schweikhard, A. Schwenk, C. Seiffert, J. Simonis *et al.*, Precision Mass Measurements of  $^{58-63}\text{Cr}$ : Nuclear Collectivity Towards the  $N = 40$  Island of Inversion, *Phys. Rev. Lett.* **120**, 232501 (2018).
- [16] Z. Meisel, S. George, S. Ahn, D. Bazin, B. A. Brown, J. Browne, J. F. Carpino, H. Chung, R. H. Cyburt, A. Estradé, M. Famiano, A. Gade, C. Langer, M. Matoš, W. Mittig, F. Montes, D. J. Morrissey, J. Pereira, H. Schatz, J. Schatz *et al.*, Nuclear mass measurements map the structure of atomic nuclei and accreting neutron stars, *Phys. Rev. C* **101**, 052801(R) (2020).
- [17] C. Jesch, T. Dickel, W. R. Plaß, D. Short, S. Ayet San Andres, J. Dilling, H. Geissel, F. Greiner, J. Lang, K. G. Leach, W. Lippert, C. Scheidenberger, and M. I. Yavor, The MR-TOF-MS isobar

- separator for the TITAN facility at TRIUMF, *Hyperfine Interact.* **235**, 97 (2015).
- [18] T. Miyagi, S. R. Stroberg, J. D. Holt, and N. Shimizu, Ab initio multishell valence-space Hamiltonians and the island of inversion, *Phys. Rev. C* **102**, 034320 (2020).
- [19] J. Dilling, R. Baartman, P. Bricault, M. Brodeur, L. Blomeley, F. Buchinger, J. Crawford, J. R. Crespo López-Urrutia, P. Delheij, M. Froese, G. P. Gwinner, Z. Ke, J. K. Lee, R. B. Moore, V. Ryjkov, G. Sikler, M. Smith, J. Ullrich, and J. Vaz, Mass measurements on highly charged radioactive ions, a new approach to high precision with TITAN, *Int. J. Mass Spectrom.* **251**, 198 (2006).
- [20] G. C. Ball, G. Hackman, and R. Krücken, The TRIUMF-ISAC facility: Two decades of discovery with rare isotope beams, *Phys. Scr.* **91**, 093002 (2016).
- [21] J. Lassen, R. Li, S. Raeder, X. Zhao, T. Dekker, H. Heggen, P. Kunz, C. D. P. Levy, M. Mostamand, A. Teigelhöfer, and F. Ames, Current developments with TRIUMF's titanium-sapphire laser based resonance ionization laser ion source, *Hyperfine Interact.* **238**, 33 (2017).
- [22] T. Brunner, M. J. Smith, M. Brodeur, S. Ettenauer, A. T. Gallant, V. V. Simon, A. Chaudhuri, A. Lapierre, E. Mané, R. Ringle, M. C. Simon, J. A. Vaz, P. Delheij, M. Good, M. R. Pearson, and J. Dilling, TITAN's digital RFQ ion beam cooler and buncher, operation and performance, *Nucl. Instrum. Methods Phys. Res., Sect. A* **676**, 32 (2012).
- [23] H. Wollnik and M. Przewloka, Time-of-flight mass spectrometers with multiply reflected ion trajectories, *Int. J. Mass Spectrom. Ion Processes* **96**, 267 (1990).
- [24] W. R. Plaß, T. Dickel, and C. Scheidenberger, Multiple-reflection time-of-flight mass spectrometry, *Int. J. Mass Spectrom.* **349-350**, 134 (2013).
- [25] M. Reiter, S. A. S. Andrés, J. Bergmann, T. Dickel, J. Dilling, A. Jacobs, A. Kwiatkowski, W. Plaß, C. Scheidenberger, D. Short, C. Will, C. Babcock, E. Dunling, A. Finlay, C. Hornung, C. Jesch, R. Klawitter, B. Kootte, D. Lascar, E. Leistenschneider *et al.*, Commissioning and performance of TITAN's multiple-reflection time-of-flight mass-spectrometer and isobar separator, *Nucl. Instrum. Methods Phys. Res., Sect. A* **1018**, 165823 (2021).
- [26] D. Stresau, K. Hunter, W. Shiels, P. Raffin, and Y. Benari, A New Class of Robust Sub-nanosecond TOF Detectors with High Dynamic Range, 54th ASMS Conference on Mass Spectroscopy (2006).
- [27] T. Dickel, M. I. Yavor, J. Lang, W. R. Plaß, W. Lippert, H. Geissel, and C. Scheidenberger, Dynamical time focus shift in multiple-reflection time-of-flight mass spectrometers, *Int. J. Mass Spectrom.* **412**, 1 (2017).
- [28] T. Dickel, W. R. Plaß, W. Lippert, J. Lang, M. I. Yavor, H. Geissel, and C. Scheidenberger, Isobar separation in a multiple-reflection time-of-flight mass spectrometer by mass-selective re-trapping, *J. Am. Soc. Mass Spectrom.* **28**, 1079 (2017).
- [29] S. Beck, B. Kootte, I. Dedes, T. Dickel, A. A. Kwiatkowski, E. M. Lykiardopoulou, W. R. Plaß, M. P. Reiter, C. Andreoiu, J. Bergmann, T. Brunner, D. Curien, J. Dilling, J. Dudek, E. Dunling, J. Flowerdew, A. Gaamouci, L. Graham, G. Gwinner, A. Jacobs *et al.*, Mass Measurements of Neutron-Deficient Yb Isotopes and Nuclear Structure at the Extreme Proton-Rich Side of the  $N = 82$  Shell, *Phys. Rev. Lett.* **127**, 112501 (2021).
- [30] S. Ayet San Andrés, C. Hornung, J. Ebert, W. R. Plaß, T. Dickel, H. Geissel, C. Scheidenberger, J. Bergmann, F. Greiner, E. Haettner, C. Jesch, W. Lippert, I. Mardor, I. Miskun, Z. Patyk, S. Pietri, A. Pihkteleev, S. Purushothaman, M. P. Reiter, A.-K. Rink *et al.*, High-resolution, accurate multiple-reflection time-of-flight mass spectrometry for short-lived, exotic nuclei of a few events in their ground and low-lying isomeric states, *Phys. Rev. C* **99**, 064313 (2019).
- [31] T. Dickel, S. Ayet San Andrés, S. Beck, J. Bergmann, J. Dilling, F. Greiner, C. Hornung, A. Jacobs, G. Kripko-Koncz, A. A. Kwiatkowski, E. Leistenschneider, A. Pihkteleev, W. R. Plaß, M. P. Reiter, C. Scheidenberger, C. Will, and the TITAN Collaboration, Recent upgrades of the multiple-reflection time-of-flight mass spectrometer at TITAN, TRIUMF, *Hyperfine Interact.* **240**, 62 (2019).
- [32] S. Purushothaman, S. Ayet San Andrés, J. Bergmann, T. Dickel, J. Ebert, H. Geissel, C. Hornung, W. R. Plaß, C. Rappold, C. Scheidenberger, Y. K. Tanaka, and M. I. Yavor, Hyper-EMG: A new probability distribution function composed of Exponentially Modified Gaussian distributions to analyze asymmetric peak shapes in high-resolution time-of-flight mass spectrometry, *Int. J. Mass Spectrom.* **421**, 245 (2017).
- [33] S. F. Paul, emgfit - Fitting of time-of-flight mass spectra with hyper-EMG models (v0.4.0), (2021), Zenodo, <https://doi.org/10.5281/zenodo.4731153>.
- [34] A. Jacobs, Master's thesis, University of British Columbia, 2019.
- [35] L. Canete, S. Giraud, A. Kankainen, B. Bastin, F. Nowacki, A. Poves, P. Ascher, T. Eronen, V. Alcindor, A. Jokinen, A. Khanam, I. D. Moore, D. A. Nesterenko, F. De Oliveira Santos, H. Penttilä, C. Petrone, I. Pohjalainen, A. de Roubin, V. A. Rubchenya, M. Vilen *et al.*, Precision mass measurements of  $^{67}\text{Fe}$  and  $^{69,70}\text{Co}$ : Nuclear structure toward  $N = 40$  and impact on  $r$ -process reaction rates, *Phys. Rev. C* **101**, 041304(R) (2020).
- [36] M. Wang, W. Huang, F. Kondev, G. Audi, and S. Naimi, The AME 2020 atomic mass evaluation (II). Tables, graphs and references, *Chin. Phys. C* **45**, 030003 (2021).
- [37] F. Kondev, M. Wang, W. Huang, S. Naimi, and G. Audi, The NUBASE2020 evaluation of nuclear physics properties, *Chin. Phys. C* **45**, 030001 (2021).
- [38] I. Mukul, C. Andreoiu, J. Bergmann, M. Brodeur, T. Brunner, K. A. Dietrich, T. Dickel, I. Dillmann, E. Dunling, D. Fusco, G. Gwinner, C. Izzo, A. Jacobs, B. Kootte, Y. Lan, E. Leistenschneider, E. M. Lykiardopoulou, S. F. Paul, M. P. Reiter, J. L. Tracy *et al.*, Examining the nuclear mass surface of Rb and Sr isotopes in the  $A \approx 104$  region via precision mass measurements, *Phys. Rev. C* **103**, 044320 (2021).
- [39] B. Pritychenko, M. Birch, B. Singh, and M. Horoi, Tables of  $E2$  transition probabilities from the first  $2^+$  states in even-even nuclei, *At. Data Nucl. Data Tables* **107**, 1 (2016).
- [40] P. Möller, A. Sierk, T. Ichikawa, and H. Sagawa, Nuclear ground-state masses and deformations: FRDM(2012), *At. Data Nucl. Data Tables* **109-110**, 1 (2016).
- [41] S. Goriely, N. Chamel, and J. M. Pearson, Hartree-Fock-Bogoliubov nuclear mass model with 0.50 MeV accuracy based on standard forms of Skyrme and pairing functionals, *Phys. Rev. C* **88**, 061302(R) (2013).
- [42] J. M. Daugas, I. Matea, J.-P. Delaroche, M. Pfützner, M. Sawicka, F. Becker, G. Bélier, C. R. Bingham, R. Borcea, E. Bouchez, A. Buta, E. Dragulescu, G. Georgiev, J. Giovannazzo, M. Girod, H. Grawe, R. Grzywacz, F. Hammache, F. Ibrahim, M. Lewitowicz *et al.*,  $\beta$ -decay measurements for  $N > 40$  Mn

- nuclei and inference of collectivity for neutron-rich Fe isotopes, *Phys. Rev. C* **83**, 054312 (2011).
- [43] P. Walker and Z. Podolyák, 100 years of nuclear isomers—then and now, *Phys. Scr.* **95**, 044004 (2020).
- [44] E. Leistenschneider, M. P. Reiter, S. Ayet San Andrés, B. Kootte, J. D. Holt, P. Navrátil, C. Babcock, C. Barbieri, B. R. Barquest, J. Bergmann, J. Bollig, T. Brunner, E. Dunling, A. Finlay, H. Geissel, L. Graham, F. Greiner, H. Hergert, C. Hornung, C. Jesch *et al.*, Dawning of the  $N = 32$  Shell Closure Seen through Precision Mass Measurements of Neutron-Rich Titanium Isotopes, *Phys. Rev. Lett.* **120**, 062503 (2018).
- [45] S. R. Stroberg, J. D. Holt, A. Schwenk, and J. Simonis, *Ab Initio* Limits of Atomic Nuclei, *Phys. Rev. Lett.* **126**, 022501 (2021).
- [46] H. Hergert, S. K. Bogner, T. D. Morris, A. Schwenk, and K. Tsukiyama, The in-medium similarity renormalization group: A novel *ab initio* method for nuclei, *Phys. Rep.* **621**, 165 (2016).
- [47] S. R. Stroberg, A. Calci, H. Hergert, J. D. Holt, S. K. Bogner, R. Roth, and A. Schwenk, Nucleus-Dependent Valence-Space Approach to Nuclear Structure, *Phys. Rev. Lett.* **118**, 032502 (2017).
- [48] S. R. Stroberg, S. K. Bogner, H. Hergert, and J. D. Holt, Non-empirical interactions for the nuclear shell model: An update, *Annu. Rev. Nucl. Part. Sci.* **69**, 307 (2019).
- [49] K. Hebeler, S. K. Bogner, R. J. Furnstahl, A. Nogga, and A. Schwenk, Improved nuclear matter calculations from chiral low-momentum interactions, *Phys. Rev. C* **83**, 031301(R) (2011).
- [50] J. Simonis, S. R. Stroberg, K. Hebeler, J. D. Holt, and A. Schwenk, Saturation with chiral interactions and consequences for finite nuclei, *Phys. Rev. C* **96**, 014303 (2017).
- [51] T. D. Morris, J. Simonis, S. R. Stroberg, C. Stumpf, G. Hagen, J. D. Holt, G. R. Jansen, T. Papenbrock, R. Roth, and A. Schwenk, Structure of the Lightest Tin Isotopes, *Phys. Rev. Lett.* **120**, 152503 (2018).
- [52] T. Miyagi, S. R. Stroberg, P. Navrátil, K. Hebeler, and J. D. Holt, Converged *ab initio* calculations of heavy nuclei, *Phys. Rev. C* **105**, 014302 (2022).
- [53] X. Xu, M. Wang, K. Blaum, J. D. Holt, Y. A. Litvinov, A. Schwenk, J. Simonis, S. R. Stroberg, Y. H. Zhang, H. S. Xu, P. Shuai, X. L. Tu, X. H. Zhou, F. R. Xu, G. Audi, R. J. Chen, X. C. Chen, C. Y. Fu, Z. Ge, W. J. Huang *et al.*, Masses of neutron-rich  $^{52-54}\text{Sc}$  and  $^{54,56}\text{Ti}$  nuclides: The  $N = 32$  subshell closure in scandium, *Phys. Rev. C* **99**, 064303 (2019).
- [54] E. Leistenschneider, E. Dunling, G. Bollen, B. A. Brown, J. Dilling, A. Hamaker, J. D. Holt, A. Jacobs, A. A. Kwiatkowski, T. Miyagi, W. S. Porter, D. Puentes, M. Redshaw, M. P. Reiter, R. Ringle, R. Sandler, C. S. Sumithrarachchi, A. A. Valverde, and I. T. Yandow, Precision Mass Measurements of Neutron-Rich Scandium Isotopes Refine the Evolution of  $N = 32$  and  $N = 34$  Shell Closures, *Phys. Rev. Lett.* **126**, 042501 (2021).
- [55] N. Shimizu, T. Mizusaki, Y. Utsuno, and Y. Tsunoda, Thick-restart block Lanczos method for large-scale shell-model calculations, *Comput. Phys. Commun.* **244**, 372 (2019).
- [56] S. R. Stroberg, <https://github.com/ragnarstroberg/imsrg>.